Anomalous Stiffening of a Conjugated Polymer During Electrochemical Oxidation

ADVANCED FUNCTIONAL MATERIALS
www.afm-journal.de

Anomalous Stiffening of a Conjugated Polymer During Electrochemical Oxidation

*Judith Pons i Tarrés, Di Zhu, Chiara Musumeci, Youngseok Kim, Dilara Meli, Hang Yu, Meghna Jha, Bryan D. Paulsen, Ruiheng Wu, Joost Kimpel, Zachary Laswick, Sri Harish Kumar Paleti, Yadong Zhang, Stephen Barlow, Seth R. Marder, Jenny Nelson, Jonathan Rivnay, and Christian Müller**

The mechanical mismatch between semiconductors and biological tissues can be a challenge for the development of conformal bioelectronics. Organic mixed ionic-electronic conductors (OMIECs) such as conjugated polymers with oligoether side chains are promising materials due to their low stiffness, which may minimize adverse immune reactions and thus promote biocompatibility. However, significant volume changes during electrochemical cycling—driven by ion and water ingression and expulsion—can lead to drastic changes in stiffness, complicating device-tissue mechanical matching across redox states. Here, the electromechanical response of a thienothiophene-based conjugated polymer with triethylene glycol side chains is investigated. Electrochemical nanoindentation and atomic force microscopy reveal a modest and reversible increase in elastic modulus at room temperature from ≈70 to more than 120 MPa upon electrochemical oxidation. This unusual mechanical stability is attributed to a reversible increase in π-stacking that compensates for swelling-induced softening. These findings demonstrate that it is feasible to design OMIEC materials with stable mechanical properties across redox states, opening new possibilities for compliant and tissue-matched bioelectronic interfaces that remain mechanically invariant during operation.

1. Introduction

The integration of electronics with biological systems requires materials that can bridge the mechanical mismatch between rigid electronic components and soft biological tissues, which, together with unconventional device architectures, can facilitate truly conformal designs.[1] It is desirable that the material in contact with a tissue or biological material shows as close as possible resemblance in terms of stiffness, meaning that materials with a wide range of elastic moduli are needed, ranging from 1 kPa to more than 10 GPa.[2–5] Conjugated polymers have emerged as versatile candidates because they combine a promising electrochemical response with biocompatibility as well as a broad portfolio of mechanical properties, making them interesting for a wide range of applications from bioelectronics to wearable devices.[6,7]

The (bending) stiffness of a polymer film depends on both the elastic modulus of the material as well as its thickness,[8] and if the latter is fixed by a certain device architecture (e.g., solar cell, transistor, etc.) then the choice of material will determine the stiffness (*stiff* and *soft* are here used to describe a material with a high and low elastic modulus, respectively). The elastic modulus of a conjugated polymer can be tuned by selecting the right type of repeat unit and side chain, by selecting a suitable degree of polymerization, and by the choice of processing method. For example,

J. Pons i Tarrés, D. Zhu, Y. Kim, M. Jha, J. Kimpel, S. H. K. Paleti, C. Müller
Department of Chemistry and Chemical Engineering
Chalmers University of Technology
Gothenburg 41296, Sweden
E-mail: christian.muller@chalmers.se

C. Musumeci
Department of Science and Technology
Laboratory of Organic Electronics
Linköping University
Norrköping 60174, Sweden

B. D. Paulsen, Z. Laswick, J. Rivnay
Department of Biomedical Engineering
Northwestern University
Evanston, IL 60208, USA

H. Yu, J. Nelson
Department of Physics and Centre for Processable Electronics
Imperial College London
London SW7 2AZ, UK

The ORCID identification number(s) for the author(s) of this article can be found under https://doi.org/10.1002/adfm.202519980

DOI: 10.1002/adfm.202519980

polymers with an all-thiophene backbone and oligoether or long alkyl side chains tend to feature a low elastic modulus of typically 1–100 MPa at room temperature, while repeat units comprising fused-ring aromatics and short side chains, as well as side-chain free backbones, result in stiff materials with elastic moduli exceeding 1 GPa.[7,9–11]

For bioelectronics, conjugated polymers with oligoether side chains are particularly promising because they combine a high electronic and ionic mobility with a relatively low stiffness,[7,12] meaning that they are potentially compliant with a wide range of tissues. These organic mixed ionic-electronic conductors (OMIECs) tend to take up water when they are in contact with an aqueous electrolyte (passive swelling) and undergo additional active swelling upon electrochemical oxidation or reduction.[8] In case of accumulation mode materials, electronic charges are introduced into the initially neutral polymer backbone via the working electrode, which are usually compensated by counterions that ingress from the electrolyte, accompanied by a hydration shell.[13,14] As a result, considerable active swelling can occur. For several polythiophenes with oligoether side chains, active swelling upon oxidation by at least 100% has been reported,[15,16] reaching a reversible volume change of up to 300% in one case (all studies used a 0.01 M KCl aqueous electrolyte).[17] During subsequent reduction, electronic charges are removed from the backbone and, at the same time, ions and water are expelled from the polymer matrix, resulting in volume contraction.

Electrochemical oxidation can affect a conjugated polymer in different ways, which can have opposing effects on the elastic modulus. Stiffening of the backbone, enhanced π-stacking and polaron-counterion interactions are likely to increase the elastic modulus, while plasticization and swelling through the uptake of counterions and solvent molecules can be expected to soften the polymer.[8] Given that OMIEC materials tend to experience considerable swelling when aqueous but also organic electrolytes are used, an overall reduction in elastic modulus can be anticipated.[8] For example, a reduction in stiffness has been observed for side-chain-free poly(3,4-propylenedioxythiophene), which experiences a decrease in elastic modulus from ≈800 to 400 MPa upon oxidation using 1 M $LiPF_6$ in propylene carbonate as the electrolyte, measured with nanoindentation.[18] Likewise, dynamic tensile deformation revealed a decrease in the elastic modulus of polypyrrole from 1 to 0.8 GPa upon oxidation using aqueous $NaPF_6$ as the electrolyte.[19] Stavrinidou et al. have recently reported a much larger relative change in elastic modulus for a polythiophene with tetraethylene glycol side chains from 68 MPa in the neat state down to ≈2 MPa upon active swelling using a 0.1 M KCl aqueous electrolyte (and 0.4 MPa in case of a 0.01 M KCl aqueous electrolyte), measured with electrochemical atomic force microscopy (EC-AFM).[13]

These significant changes in stiffness upon oxidation are likely to complicate the use of OMIEC materials for the design of electrochemical devices that maintain the same mechanical compliance and whose elastic modulus matches that of a specific type of cell culture or biological tissue throughout a complete oxidation/reduction cycle. This is important because many cell cultures and tissues show a preference for substrates with a specific elastic modulus.[20,21] It would be advantageous if polymers could be identified that do not significantly change their mechanical response, since this would allow the design of electrochemical devices with an elastic modulus that is less dependent on the oxidation level. To realize this type of invariant mechanical response, it would be necessary to compensate for the swelling-induced reduction in elastic modulus.

Polythiophenes with oligoether side chains have a low glass transition temperature $T_g < -30$ °C and therefore a low elastic modulus at room temperature.[12,22] For example, static tensile deformation revealed that a polythiophene with triethylene glycol side chains has a Young's modulus of 76 MPa at room temperature, which increases more than 10-fold upon chemical doping with 2,3,5,6-tetrafluoro-7,7,8,8-tetracyanoquinodimethane (F_4TCNQ), likely because of the accompanied increase in T_g to 1 °C as well as an increase in π-stacking.[22] Instead, a thienothiophene-based copolymer with triethylene glycol side chains, p(g_3TT-T2) (see **Figure 1a** for chemical structure), has a higher Young's modulus of more than 300 MPa at room temperature when measured with static tensile deformation, likely because of its higher $T_g = -5$ °C (unpublished result). We therefore hypothesized that a polymer such as p(g_3TT-T2) with relatively rigid repeat units compared to an all-thiophene backbone may display a less pronounced change in modulus upon oxidation.

Here, we show that the elastic modulus of a thienothiophene-based copolymer with triethylene glycol side chains, p(g_3TT-T2) (see Figure 1a for chemical structure), features a slight increase in elastic modulus from ≈70 to more than 120 MPa upon electrochemical oxidation using a NaCl based aqueous electrolyte, which only shows a weak dependence on the electrolyte concentration. This is because swelling by the aqueous electrolyte is counteracted by a reversible decrease in π-stacking upon oxidation. Our results suggest that it is possible to design OMIEC materials that undergo minimal changes in modulus during electrochemical oxidation/reduction cycles.

2. Results and Discussion

In a first set of experiments, we characterized p(g_3TT-T2) films with cyclic voltammetry (CV). We used a three-electrode configuration consisting of 1) an indium tin oxide (ITO) working electrode on which a 40 nm thin film of p(g_3TT-T2) was spin-coated, 2) a platinum counter electrode, and 3) an Ag/AgCl reference electrode (Figure 1b; see Experimental for details). A physiologically relevant aqueous electrolyte containing 0.1 M NaCl

Y. Zhang, S. Barlow, S. R. Marder
Renewable and Sustainable Energy Institute (RASEI)
University of Colorado Boulder
Boulder, CO 80309, USA
S. R. Marder
Departments of Chemical and Biological Engineering and of Chemistry
University of Colorado Boulder
Boulder, CO 80309, USA
D. Meli, J. Rivnay
Department of Material Science and Engineering
Northwestern University
Evanston, IL 60208, USA
R. Wu
Department of Chemistry
Northwestern University
Evanston, IL 60208, USA

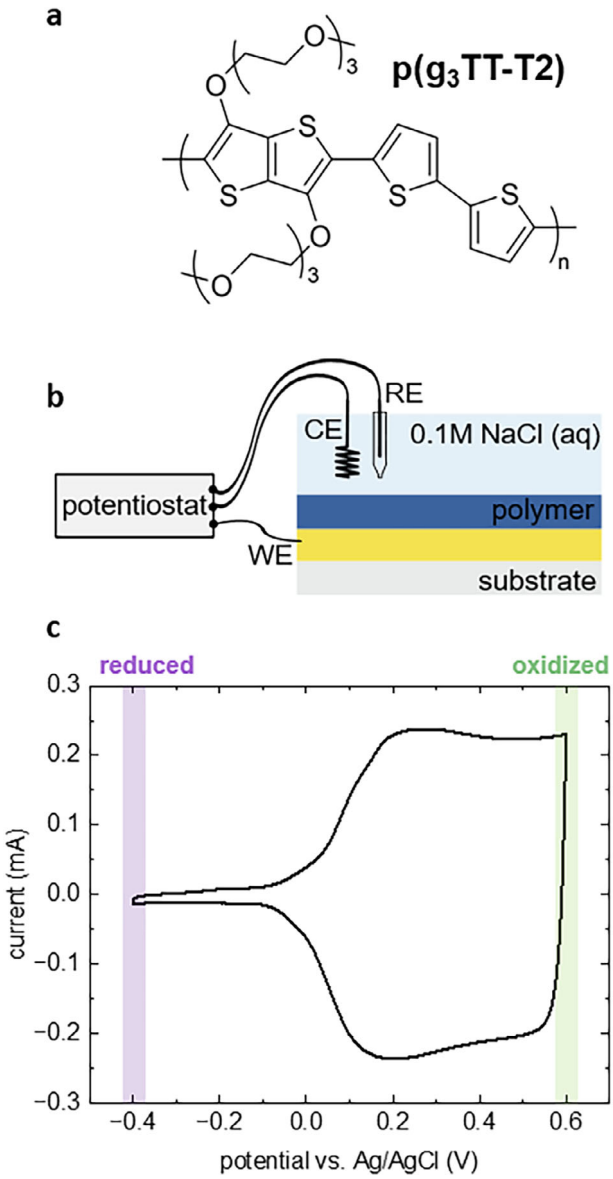

Figure 1. Cyclic Voltammetry. a) Chemical structure of p(g_3TT-T2), b) schematic of the setup used for cyclic voltammetry (CV), electrochemical nanoindentation (EC-nanoindentation) and electrochemical atomic force microscopy (EC-AFM) comprising a bottom working electrode (WE) as well as a counter electrode (CE) and a reference electrode (RE) submerged in a NaCl aqueous electrolyte, and c) cyclic voltammogram measured at a scan rate of 100 mV s^{-1} using a 0.1 M NaCl aqueous electrolyte and a Ag/AgCl reference electrode.

was used. Cyclic voltammograms were recorded during repeated cycling between −0.4 V and +0.6 V versus Ag/AgCl where the polymer is completely reduced and highly oxidized, respectively (Figure 1c). Repeated cycling resulted in voltammograms with the same shape, indicating that the polymer can be reversibly oxidized/reduced (Figure S1, Supporting Information). Voltammograms reveal an oxidation onset potential E_{ox} = +0.05 V versus Ag/AgCl, which suggests that the polymer has an ionization energy IE = E_{ox} + 4.64 eV = 4.69 eV.[23] Integration of the current up to +0.6 V versus Ag/AgCl yielded a total charge of $q = 6 \cdot 10^{-4}$ C, which implies that the oxidized film with a dry film volume of $5.7 \cdot 10^{-6}$ cm^3 reaches a charge density of $n = 7 \cdot 10^{20}$ cm^{-3}, assuming that oxidation of the polymer is the only redox process. Evidently, the polymer is highly oxidized at +0.6 V versus Ag/AgCl.

To facilitate nanoindentation experiments, we investigated how micrometer-thick films respond to repeated electrochemical oxidation/reduction cycles. Thick films are needed so that the tip does not sense the underlying substate as it indents the film. In case of micrometer-thick films drop-cast on ITO, we observed delamination already after the first oxidation-reduction cycle (**Figure 2**). Wang et al. have shown that delamination during electrochemical cycling occurs once the energy release rate due to swelling, which scales with film thickness, exceeds the interfacial toughness.[18] Hence, it can be anticipated that delamination of micrometer-thick p(g_3TT-T2) films can be mitigated by improving bonding to the underlying ITO substrate. In a previous study, some of us avoided delamination during electrochemical cycling by modifying a polymer/substrate interface with a phosphonic acid functionalized with a fluorinated aryl azide.[24] The phosphonic acid group is known to strongly bind to metal oxides,[25] while photolysis of fluorinated aryl azides affords reactive nitrenes that insert into C—H bonds,[26] in this case, those of the polymer. Here, we use a similar approach based on a phosphonic acid functionalized with a 3-(trifluoromethyl)-3-aryldiazirine (diazirine PA), a group that is known to be photolyzed to carbenes that, like the above-mentioned azides, can insert into C—H bonds.[27] Diazirine PA was synthesized (see Supporting Information for synthetic details) and deposited onto ITO as described in the experimental section, followed by spin coating of the polymer. The stack was then irradiated with UV light through the glass substrate to initiate the formation of reactive carbenes (Figure 2). We observe that UV-irradiated p(g_3TT-T2) films on diazirine PA modified ITO do not experience delamination upon electrochemical cycling (Figure 2), consistent with covalent tethering of the polymer film to the ITO electrode. X-ray photoelectron spectroscopy (XPS) revealed a distinct fluorine signal, which is consistent with the presence of the diazirine PA underneath the polymer film (Figure S2, Supporting Information).

Nanoindentation of 3 to 8 µm thick films on diazirine PA modified ITO was performed using a three-segment protocol consisting of 1) a loading phase during which the applied load P was gradually increased, 2) a hold phase where a constant load P_{hold} was maintained and 3) an unloading phase during which the tip was retracted (see **Figure 3a** for representative force-displacement curves). The elastic modulus was extracted either from the hold segment using creep compliance analysis (Figure 3b; Figure S3, Supporting Information; see Experimental for details) or from the unloading segment using the Oliver-Pharr method.[7] Electrochemical (EC) nanoindentation was conducted under four distinct conditions: 1) dry (neat) films, 2) passively swollen films submerged in 0.01 to 1 M NaCl aqueous electrolyte (no bias), 3) films oxidized at +0.6 V versus Ag/AgCl, and 4) films reduced at −0.4 V versus Ag/AgCl. Note that films were first oxidized/reduced ex situ and then indented through the electrolyte while continuously applying an open-circuit potential via a pseudo-reference Ag wire electrode (see Experimental for details).

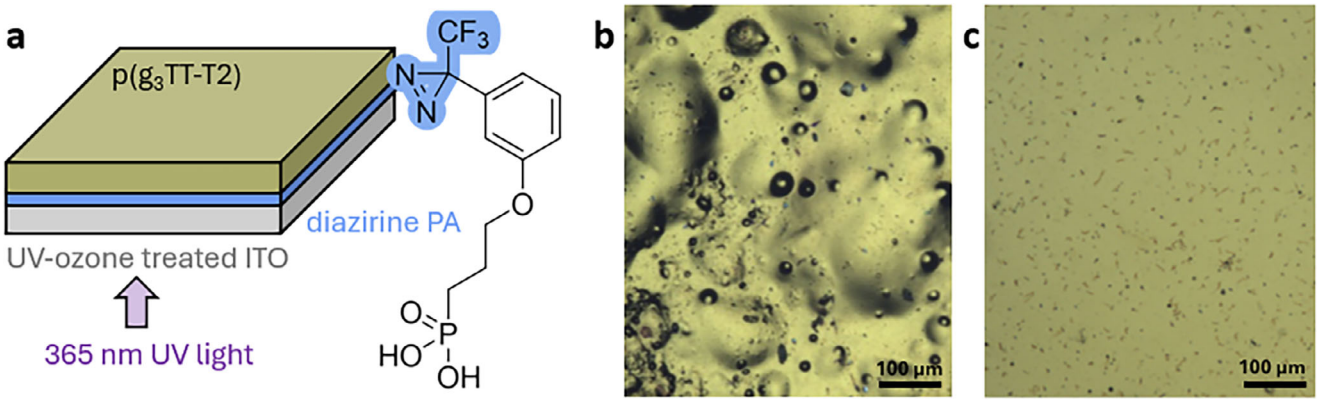

Figure 2. ITO modification. a) Schematic of ITO modification with a diazirine-functionalized phosphonic acid (diazirine PA), b) optical micrograph of p(g_3TT-T2) on ITO after the first oxidation-reduction cycle (0.1 M NaCl aqueous electrolyte; +0.6 to −0.4 V vs Ag/AgCl), and c) optical micrograph of p(g_3TT-T2) on diazirine PA-modified ITO after five oxidation-reduction cycles.

Load-displacement curves varied significantly across these conditions. For instance, during both the loading and hold phase passively swollen films are more strongly indented than oxidized films despite a similar load profile (Figure 3a), consistent with a higher stiffness in case of the latter. As a result, the creep compliance approaches a lower value for long hold times in case of oxidized films (e.g., $J = 35$ vs 105 GPa^{-1} at $t = 600$ s in Figure 3b). Overall, nanoindentation reveals a tensile elastic modulus of $E =$ (121 ± 35) MPa in case of dry films, which decreases to (73 ± 10) MPa upon immersion of films in 0.1 M NaCl aqueous electrolyte (no bias; **Figure** 4a). Strikingly, for oxidized films, which remain in 0.1 M NaCl aqueous electrolyte during the nanoindentation measurements, we observe a value of $E =$ (127 ± 25) MPa, which decreases again to (47 ± 19) MPa upon reduction (Figure 4a).

EC-AFM was used to investigate the extent to which the changes in elastic modulus observed with EC-nanoindentation for micrometer-thick films also occur in case of 200 nm thin films. The same four conditions were probed, i.e., dry (neat) films as well as passively swollen (no bias), oxidized (+0.6 V vs Ag/AgCl), and reduced (−0.4 V vs Ag/AgCl) films. EC-AFM confirmed the trend observed with EC-nanoindentation. Dry films exhibited an elastic modulus of $E =$ (171 ± 51) MPa, which decreased to (80 ± 18) MPa when passively swollen and then varied between $E =$ (253 ± 91) MPa and (144 ± 32) MPa for oxidized and reduced films, respectively (Figure 4b; see Figure S4,

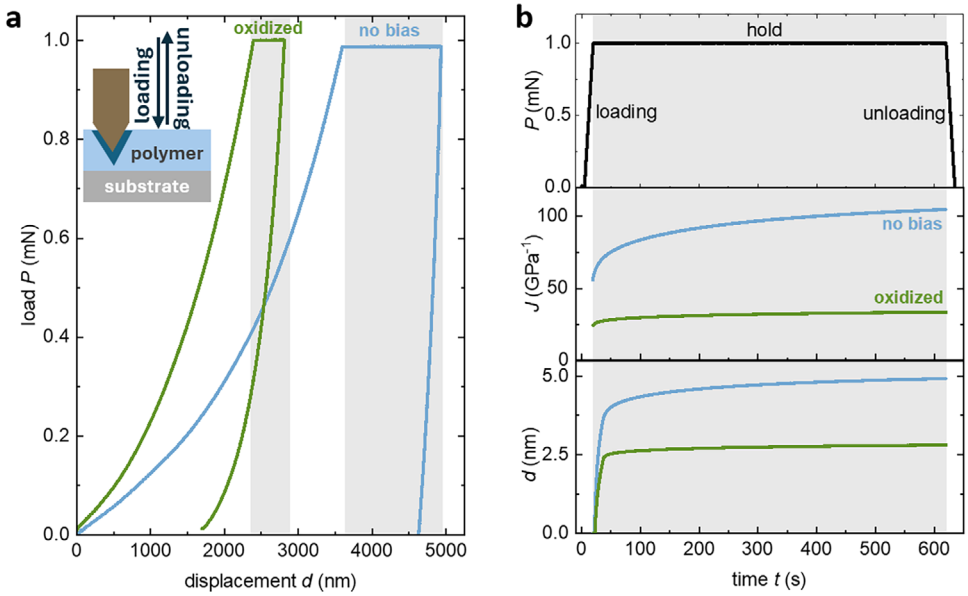

Figure 3. Electrochemical (EC)-nanoindentation measurement. a) Representative load-displacement curves recorded during EC-nanoindentation of a more than 6 μm thick p(g_3TT-T2) film covered by 0.1 M NaCl aqueous electrolyte at no bias (blue) and oxidized at +0.6 V versus Ag/AgCl (green) with the hold segments shaded in grey; b) load $P(t)$ (top panel), creep compliance $J(t)$ (middle panel) and displacement $d(t)$ (bottom panel) recorded for a film at no bias (blue) and oxidized at +0.6 V versus Ag/AgCl (green) during a load cycle composed of an initial loading and final unloading segment (loading/unloading rate $\mathbf{d}P/\mathrm{d}t = \pm 20$ µN s^{-1}) separated by a $t = 600$ s long hold segment (load $P_{hold} = 1$ mN).

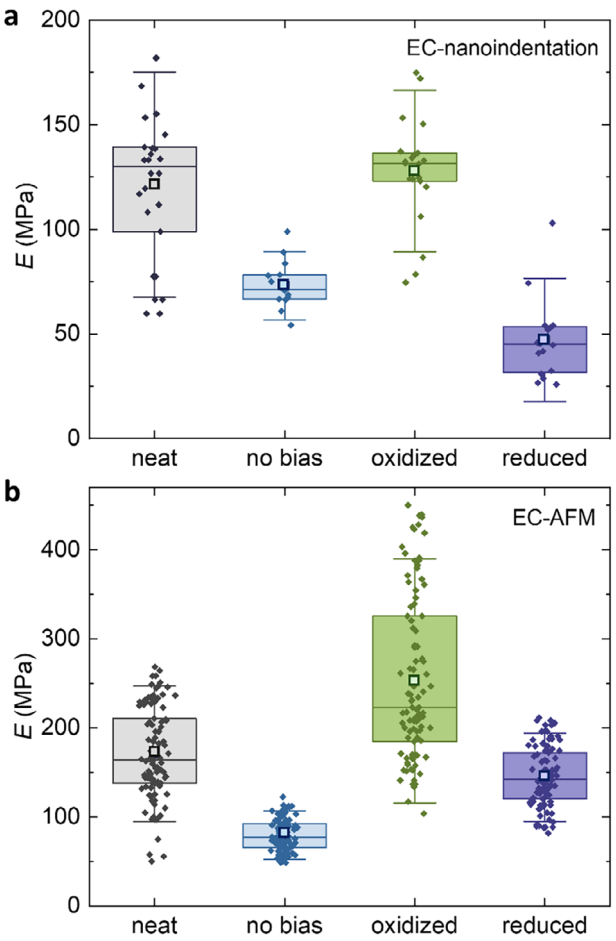

Figure 4. Elastic modulus *E* obtained from a) EC-nanoindentation of five films with a neat film thickness of 3 to 8 μm, and b) EC-AFM of a film with a neat film thickness of ≈200 nm measured without electrolyte (grey) and when covered by 0.1 M NaCl aqueous electrolyte at no bias (light blue), oxidized at +0.6 V (green) or reduced at -0.4 V versus Ag/AgCl (purple); boxes indicate the interquartile range of individual measurements (each datapoint corresponds to the mean of values obtained from 9 to 12 creep measurements in case of EC-nanoindentation and 100 single force-distance curves in case of EC-AFM) and the horizontal line inside each box indicates the median, while the overall mean is shown as a square and the standard deviation as error bars.

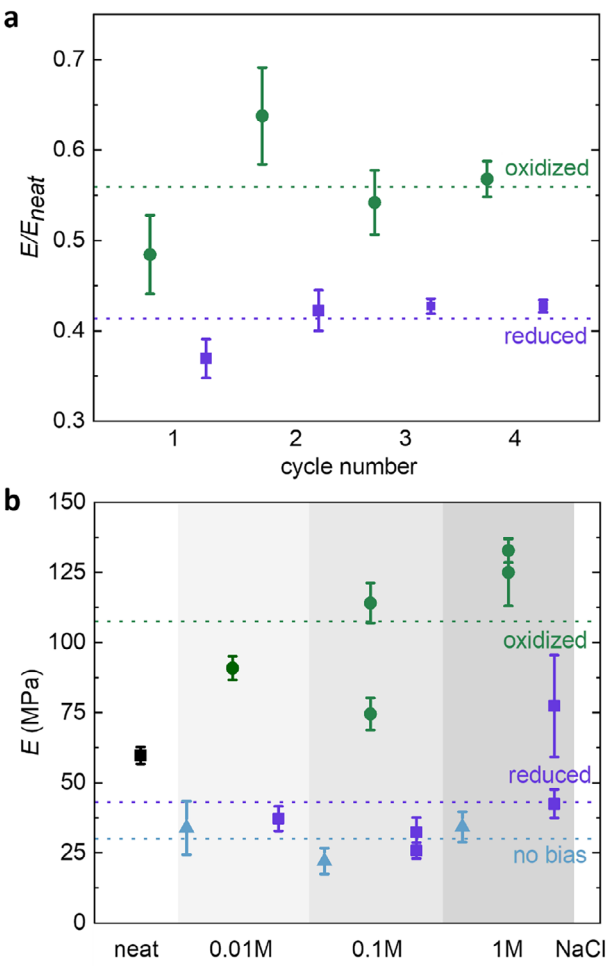

Figure 5. Cyclic EC-nanoindentation measurements and effect of electrolyte concentration. a) Relative change in elastic modulus E/E_{neat} for the same 3.5 µm thick film covered by 0.1 M NaCl aqueous electrolyte, where E_{neat} is the modulus of the neat film, upon repeated oxidation at +0.6 V (green circles) and reduction at −0.4 V versus Ag/AgCl (purple squares), measured with EC-nanoindentation and analyzed using the Oliver-Pharr method (dashed lines represent the mean of all cycles); and b) elastic modulus of the same film when measured without electrolyte (black square) or when covered by 0.01, 0.1 or 1 M NaCl aqueous electrolyte and measured without bias (light blue triangles), upon oxidation at +0.6 V (green circles) and reduction at −0.4 V versus Ag/AgCl (purple squares) using EC-nanoindentation and creep analysis (the dashed line represents the mean of all cycles). Each datapoint, i.e., circle for oxidation, triangle for no bias, and square for the neat and reduced conditions, corresponds to the mean of values obtained from 9 to 12 creep measurements with the corresponding standard deviation shown as error bars.

Supporting Information for representative load vs tip-sample separation curves).

In a further set of experiments, we investigated to which extent the observed changes in elastic modulus are reproducible across multiple redox cycles, again using a 0.1 M NaCl aqueous electrolyte. To follow relative changes in elastic modulus over multiple redox cycles, EC-nanoindentation of a 3.5 µm thick film in combination with analysis based on the Oliver-Pharr method was used. While the Oliver-Pharr method is known to overestimate the elastic modulus of polymer films due to plastic deformation and pile up of material around the nanoindenter tip,[7] it was used because measurements are significantly faster than creep analysis experiments. We find that the relative increase in elastic modulus upon oxidation and decrease upon reduction occurs for at least four redox cycles (**Figure** 5a). EC-AFM of a 200 nm thin film across seven redox cycles confirmed that the observed change in elastic modulus is reversible (Figure S5, Supporting Information).

To investigate the influence of the electrolyte concentration, EC nanoindentation experiments with 0.01, 0.1, and 1 M NaCl aqueous electrolytes were compared. To this end, a neat film, which initially exhibited an elastic modulus of (60 ± 3) MPa, was immersed in 1 M NaCl aqueous electrolyte, followed by oxidation and then reduction. This sequence was repeated with 0.1 M and finally 0.01 M NaCl aqueous electrolyte, and then measured again

while increasing the electrolyte concentration to 0.1 M and finally 1 M NaCl. In case of 0.01 and 0.1 M NaCl aqueous electrolytes, reduced films yielded values between 20 and 40 MPa, while 1 M NaCl resulted in somewhat higher values (Figure 5b). The oxidized film featured a higher modulus of 70 to 130 MPa, with the film oxidized using 1 M NaCl featuring the highest elastic modulus of $E = (129 \pm 9)$ MPa (Figure 5b).

To elucidate the influence of electrolyte concentration, which is known to influence the degree of swelling of OMIECs,[28] electrochemical quartz-crystal microbalance (EQCM) measurements were performed in 0.01, 0.1, and 1 M NaCl aqueous electrolyte over seven redox cycles. Dilute aqueous electrolytes comprising 0.01 or 0.1 M NaCl gave rise to reversible mass changes. Each oxidation half-cycle was characterized by an initial decrease in mass followed by a mass uptake between −0.2 to +0.6 V versus Ag/AgCl, while reduction half-cycles showed the reverse behavior with mass loss followed by mass uptake (**Figure 6**a,b). We argue that Na^+ cations enter fully reduced films, resulting in a slight mass uptake, which are expelled upon oxidation, while at the same time Cl^- anions enter the film. In contrast, in case of 1 M NaCl aqueous electrolyte, polymer films undergo irreversible swelling, indicative of structural changes and/or incomplete recovery during cycling, i.e., some ions and/or water remain in the reduced film, as evidenced by the increase in residual mass change at the end of each subsequent redox cycle (Figure 6a,b). The irreversible swelling in the case of 1 M NaCl aqueous electrolyte may explain why we observe a slightly higher modulus upon both oxidation and reduction compared with values observed when using a less concentrated electrolyte (see Figure 5b)—the polymer thin film may undergo cumulative stiffening over consecutive redox cycles. Comparison of the reduced and oxidized state at −0.4 V and +0.6 V versus Ag/AgCl yields a reversible mass uptake of $\Delta m/m_{neat} \approx 30\%$ in case of 0.01 and 0.1 M NaCl where $\Delta m = m(t) - m(t = 0)$ is the change in mass of the polymer thin films during active swelling and m_{neat} is the mass of the pristine dry film (neat). Instead, for 1 M NaCl there is a gradual increase in mass uptake with each redox cycle due to incomplete recovery (see Figure 6b for EQCM of a ≈100 nm thin film and Figure S6, Supporting Information for EQCM with dissipation monitoring (EQCM-D) of 300 nm thick films, which indicated a similar degree of swelling). Note that the active swelling during each redox cycle occurs in addition to the passive swelling that a neat film experiences once it is placed in the electrolyte, which is ≈(15.7 ± 0.3)%, as judged by the increase in weight of a compression-molded 0.5 mm thick film that had been submerged in 0.1 M NaCl aqueous electrolyte for 24 h. The degree of swelling of p(g_3TT-T2) is slightly lower than values reported for other thienothiophene-based materials,[28] but in contrast to previous reports, the electrolyte concentration appears to have little influence on the degree of swelling. Analysis of cyclic voltammograms suggested that p(g_3TT-T2) films oxidized at +0.6 V versus Ag/AgCl have a charge-carrier density of $\approx n = 7 \cdot 10^{20}$ cm^{-3}, meaning that ≈58% of all repeat units of the polymer are oxidized since neat p(g_3TT-T2) has a density of $\rho = 1.2$ g cm^{-3} (unpublished result) and therefore $1.2 \cdot 10^{21}$ repeat units per cm^{-3}. Assuming each hole is compensated by one Cl^-, which accounts for a mass increase of only 0.58 $M_{Cl}/(M_{g_3TT-T2}) \approx 3\%$, it can be concluded that the majority of the mass increase likely occurs due to the ingression of water that accompanies Cl^- ions.

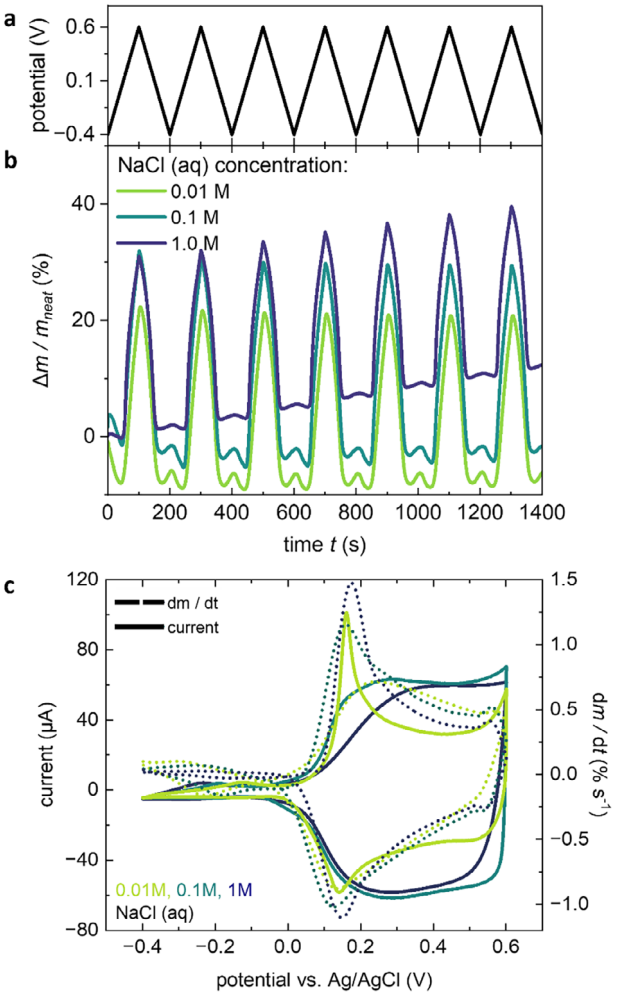

Figure 6. Electrochemical quartz crystal microbalance (EQCM) measurements. a) Applied potential profile used during the EQCM measurements; b) fractional mass change of actively swollen polymer thin films relative to their initial pristine dry states, $\Delta m/m_{neat} = [m(t) - m(t = 0)]/m_{neat}$, calculated from the EQCM measurements for ≈300 nm thick films; measurements were performed in Ar-saturated NaCl aqueous electrolytes with concentrations of 0.01, 0.1 and 1.0 M, using a fresh film for each concentration; each film underwent seven CV cycles, scanned from −0.4 to 0.6 V versus Ag/AgCl at a scan rate of 10 mV s^{-1}; and c) comparison of CV and gravimetric CV.

Swelling due to water uptake can be anticipated to soften films and therefore cannot explain the increase in elastic modulus observed upon oxidation (see Figures 4 and 5).

To assess the kinetics of ion ingression/expulsion, gravimetric cyclic voltammetry was employed. The ionic current, which scales with the time derivative of mass change, can be compared with the electronic current from CV. In case of 0.01 and 0.1 M NaCl aqueous electrolyte, there is a distinct mass expulsion peak between −0.4 and +0.05 V versus Ag/AgCl, which we attribute to the expulsion of Na^+ and its hydration sphere (Figure 6c). Mass uptake associated with the ingression of Cl^- anions and their hydration sphere starts to occur at E_{ox} = ca. +0.05 V and peaks at ≈+0.2 V, which precedes the peak in the more gradually increasing hole current. In case of 1 M NaCl aqueous electrolyte, the ionic

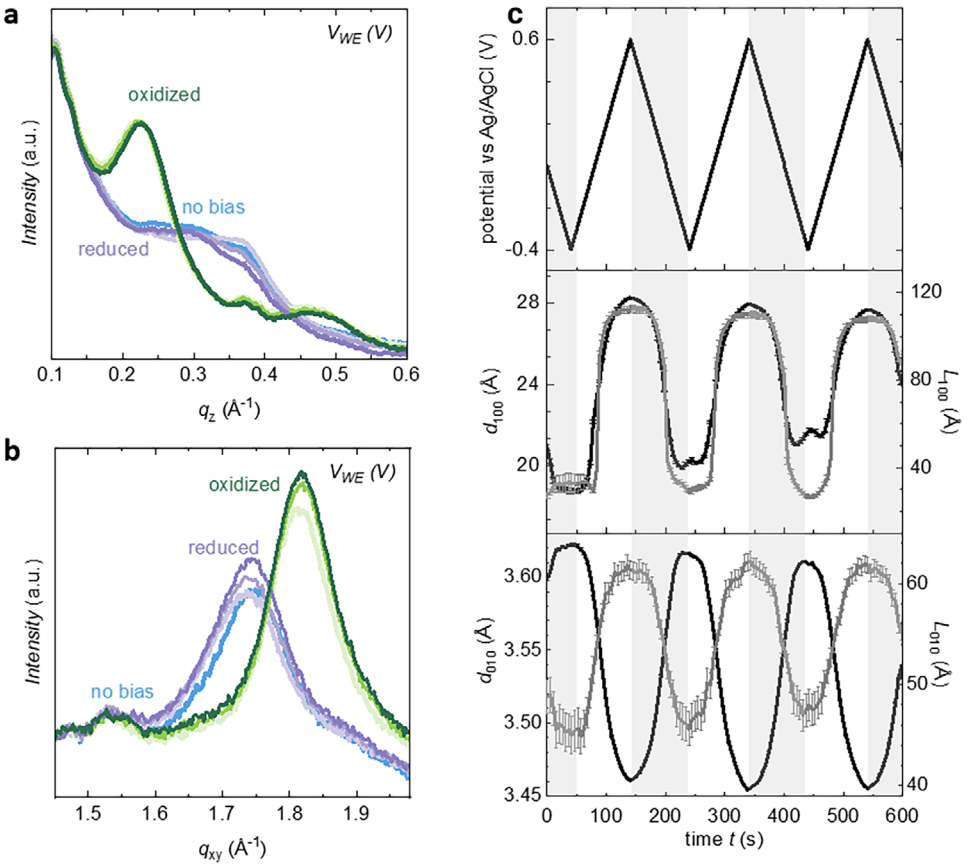

Figure 7. Operando grazing-incidence wide-angle X-ray scattering (GIWAXS) of a p(g_3TT-T2) thin film. a) Out-of-plane (100) and b) in-plane (010) scattering corresponding to lamellar and π-stacking, respectively, recorded for the same film during sequential CV cycles at +0.6 and −0.4 V versus Ag/AgCl in 0.1 M NaCl aqueous electrolyte (scan rate 10 mV s^{-1}); c) applied potential versus Ag/AgCl (top) lamellar spacing d_{100} and coherence length L_{100} (center) and π-stacking distance d_{010} and coherence length L_{010} (bottom) recorded during three redox cycles (distance in black; coherence length in grey).

and electronic currents are more closely aligned, indicating faster ion exchange kinetics and a high degree of ion-electron coupling compared to lower electrolyte concentrations.

To understand the stiffening of the polymer upon oxidation despite Cl^- ion and water uptake, operando grazing-incidence wide-angle X-ray scattering (GIWAXS) was carried out to monitor the evolution of the nanostructure during electrochemical cycling between −0.4 and +0.6 V versus Ag/AgCl. GIWAXS patterns of a passively swollen polymer film indicate an edge-on texture with an out-of-plane signal at q_z = 0.36 Å^{-1} and a distinct diffraction peak in-plane at q_{xy} = 1.74 Å^{-1}, which correspond to lamellar stacking in the side-chain direction and π-stacking of the backbone, respectively (**Figure** 7a,b). Upon oxidation, once the potential exceeds 0 V versus Ag/AgCl there is a shift of the 100 and 010 diffraction peaks to lower and higher q values, respectively, meaning that the lamellar stacking distance increases from d_{100} = 18.5 to 27.5 Å, while the π-stacking distance decreases from d_{010} = 3.6 to 3.5 Å (Figure 7c; Table S1, Supporting Information). Several previous studies dealing with chemical or electrochemical doping have rationalized the increase in lamellar stacking distance with intercalation of anions between the side chains.[29–34] In addition, both peaks become significantly sharper, indicating an increase in coherence length and therefore a considerable increase in the degree of order of oxidized p(g_3TT-T2). We argue that this increase in the degree of order (in combination with possible stiffening of the polymer backbone due to the presence of polarons) counteracts the swelling induced softening of the film (see **Figure** 8 for an illustration of the influence of passive and active swelling as well as oxidation/reduction on the nanostructure of polymer films), overall resulting in an increase in elastic modulus as observed with EC-nanoindentation and EC-AFM (Figures 4 and 5). Importantly, the observed changes in nanostructure appear mostly reversible over multiple redox cycles (Video S1, Supporting Information), consistent with softening of the polymer film upon reduction. We note that the 010 diffraction feature returns to its original position upon reduction, while the 100 peak does not fully recover (Figure 7c). We argue that a limited number of ions and/or water remain in the side-chain regions, leading to some degree of irreversible change.

3. Conclusion

We investigated the electromechanical response of the conjugated polymer p(g_3TT-T2), a thienothiophene-based OMIEC with triethylene glycol side chains, across various electrolyte

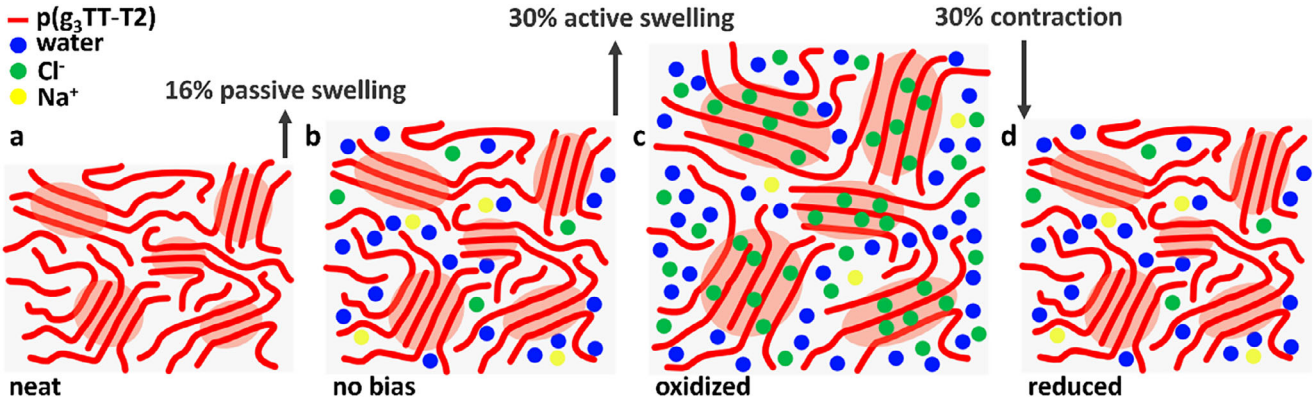

Figure 8. Illustration of the changes in nanostructure of a p(g_3TT-T2) film upon passive and active swelling/contraction with side chains omitted for clarity. a) The neat film comprising ordered (red shaded areas) and disordered domains, b) experiences 16% passive swelling when placed in a 0.1 M NaCl aqueous electrolyte, followed by c) 30% active swelling once a bias of +0.6 V versus Ag/AgCl is applied, and d) contraction once biased at −0.4 V versus Ag/AgCl.

concentrations and redox states. Electrochemical nanoindentation and atomic force microscopy revealed that polymer films exhibit a modest and reversible increase in stiffness upon oxidation, rather than the expected softening due to swelling as a result of water uptake. The elastic modulus increased from ≈70 MPa in the passively swollen state to over 120 MPa upon oxidation, with a similar trend observed for both ≈200 nm thin and 3 to 8 μm thick films. The observed changes were reversible over multiple redox cycles and only weakly depended on electrolyte concentration ranging from 0.1 to 1 M NaCl. EQCM measurements indicated a reversible mass uptake of ≈30% upon oxidation, which primarily occurred due to the uptake of water that accompanied compensating Cl^- anions. Concurrently, operando GIWAXS revealed that oxidation triggers a reversible increase in molecular order, with an increase in the coherence length of π and lamellar stacking. Hence, the oxidation-induced stiffening was attributed to the observed increase in structural order, which counteracted swelling-induced softening, overall resulting in a higher elastic modulus. In the future, it would be interesting to study how different types of electrolytes influence the mechanical response. The observed mechanical response suggests that it is possible to design OMIEC materials that stiffen despite swelling. It can be concluded that redox-active polymers with stable mechanical properties across redox states can be designed, which is essential for the realization of compliant bioelectronic devices.

4. Experimental Section

Materials: The preparation and characterization of p(g_3TT-T2) with a number-average molecular weight $M_{n,SEC}$ = 13 kg mol^{-1} and dispersity $Đ$ = 1.5, measured with size exclusion chromatography (SEC), and $M_{n,NMR}$ = 9 kg mol^{-1}, measured with high-temperature nuclear magnetic resonance (NMR),[35] was described previously.[36] The synthesis of (3-(3-(3-(trifluoromethyl)-3*H*-diazirin-3-yl)phenoxy)propyl)phosphonic acid (diazirine PA) is described in the Supporting Information (Figures S7–S15). Chloroform (analytical reagent grade) and sodium chloride (analytical reagent grade) were purchased from Thermo Fisher Scientific. Deionized water was obtained from a Milli-Q Q-POD water purification system.

Film Preparation: Substrates for nanoindentation consisted of patterned Au- or ITO-coated glass slides (obtained from Ossila) that were cleaned with deionized water, acetone, and isopropyl alcohol and then UV-ozone treated. Where indicated, cleaned ITO-coated glass slides were modified with diazirine PA by covering them with a solution of 0.3 g L^{-1} diazirine PA in 2,2,2-trifluoroethanol (TFE; Tokyo Chemical Industry) for 1 to 2 min, followed by spinning (3000 rpm, 60 s), annealing at 80 °C for 5 min, and finally washing with TFE (twice covered with TFE followed by spinning for 60 s at 3000 rpm). Films for nanoindentation with a thickness ranging from 3 to 8 μm were prepared by drop casting solutions of 20 g L^{-1} p(g_3TT-T2) in chloroform on the respective substrate. Films on diazirine PA modified ITO-coated glass slides were illuminated for 15 min from the uncoated side with UV light from a 365 nm LED lamp (Merry Change, MC-LED20, 50W, 0.5A) kept at a distance of 20 cm. For XPS, a very thin polymer film was spin-coated on diazirine PA modified ITO from a solution of 0.625 g L^{-1} p(g_3TT-T2) in chloroform. Thin films with a thickness of ≈40 nm for CV, ≈100 nm for EQCM-D and GIWAXS, ≈200 nm for EC-AFM and ≈300 nm for EQCM were spin coated from solutions of 8, 14 or 30 g L^{-1} p(g_3TT-T2) in chloroform on the following substrates: 1) ITO-coated glass slides (Ossila) for CV, 2) a cut silicon wafer (Silicon Materials Inc.) with 50 Å Cr and 450 Å Au evaporated on top (with a Kurt J Lesker PVD e-beam evaporator) for EC-AFM, 3) Au-coated quartz crystals (Biolin Scientific and Quartz PRO) for EQCM-D and EQCM, respectively, and 4) glass slides that had been spin coated with a 3 wt.% aqueous solution of poly(sodium 4-styrenesulfonate) (PSS; Sigma Aldrich) for GIWAXS. For passive swelling measurements a 0.5 mm thick p(g_3TT-T2) film was prepared by compression molding at 120 °C for 15 min at 15 kN. The film was dried in a vacuum oven at 45 °C for 24 h before measuring its dry mass. The film was then placed in 0.1 M NaCl aqueous electrolyte for 24 h, and the wet mass was measured, yielding a mass uptake of (15.7 ± 0.3)%.

X-Ray Photoelectron Spectroscopy (XPS): XPS spectra were recorded with a Versaprobe III scanning XPS system from Physical Instruments using monochromatized Al X-ray radiation (energy = 1486.6 eV) with an illuminated spot size of 100 µm^2 using a step size of 1.0 eV from 0 to 1350 eV to evaluate the overall chemical composition or 0.1 eV to investigate the chemical state of individual elements. Samples were mounted on a non-conductive adhesive. Charge compensation was ensured by a combination of an electron flood gun and an Ar^+ ion source. Prior to qualitative analysis, the binding energy scale was aligned with reference to the position of adventitious carbon, i.e., C1s = 284.8 eV.

Cyclic Voltammetry: Cyclic voltammetry (CV) was conducted with a 0.1 M NaCl aqueous electrolyte (continuously purged with nitrogen) and a three-electrode configuration (Ag/AgCl reference electrode with 3 M KCl, Pt wire counter electrode, and ITO working electrode below the polymer film; see Figure 1b) using a SP-300 electrochemical workstation from Bio-Logic. Before and during characterization, the electrolyte was purged with nitrogen gas. Voltammograms were recorded using a scan rate of 10 or 100 mV s^{-1}.

Nanoindentation: Measurements were performed at room temperature with a Hysitron TI Premier instrument from Bruker equipped with a Berkovich tip made of diamond with a half angle of $\alpha = 65.27°$ and a tip radius of 100 nm attached to a liquid-compatible stylus, calibrated with a reference quartz substrate. Prior to each measurement, the nanoindenter was left in idle condition for half an hour to reach thermal equilibrium. The creep compliance was determined by recording the change in indentation depth $h(t)$ during the hold phase at a constant load of P_{hold} according to:[7]

$$J(t) = \frac{4h^2(t)}{\pi(1-\upsilon)\cdot P_{hold}\cdot \tan\alpha} \tag{1}$$

where $\upsilon = 0.35$ is the Poisson's ratio. The shear and tensile relaxation modulus, G and E, were calculated according to:

$$G = \left.\frac{1}{J(t)}\right|_{t\gg 0} \tag{2}$$

and

$$E = 3G\cdot(1+\upsilon) \tag{3}$$

Reported values for E are the mean and standard deviation based on 9 to 12 creep measurements carried out using a loading rate of 20 μN s^{-1}, a maximum load varying from P_{hold} = 80 to 1000 μN and a hold time of 600 s. In case of cycling experiments, the Oliver-Pharr method was used to estimate E:[37]

$$E = \frac{S\left(1-\nu^2\right)\sqrt{\pi}}{2A(h)} \tag{4}$$

where $S = dP/dh$ is the stiffness calculated from the initial slope of the unloading curve and $A(h)$ is the projected area of the indentation tip. Measurements of dry films without any electrolyte were carried out at 20% relative humidity. Electrochemical (EC) nanoindentation was done by covering films with 0.01, 0.1 or 1 M NaCl aqueous electrolyte (not purged with nitrogen) contained in a reservoir defined by a 5 mm high polydimethylsiloxane (PDMS) well to which a 15 mL electrochemical cell was attached for oxidation or reduction at +0.6 and −0.4 V versus Ag/AgCl, respectively, in three-electrode configuration (Ag/AgCl reference electrode with 3 M KCl, Pt wire counter electrode and ITO or Au working electrode below the polymer film) using a SP-300 electrochemical workstation from BioLogic. Then, the sample and electrolyte reservoir (without the electrochemical cell) were transferred to the nanoindenter for EC-nanoindentation measurements. To maintain the same potential throughout the measurements an open-circuit voltage V_{oc} was applied via a pseudo-reference Ag wire electrode embedded in the PDMS spacer with $V_{oc} = E_{Ag\ wire} - E_{Ag/AgCl}$ = 0.6–0.52 V = 0.08 V.

Electrochemical Atomic Force Microscopy (EC-AFM): EC-AFM was performed with a Dimension Icon XR from Bruker. The samples were mounted in an electrochemical cell filled with 0.1 M NaCl aqueous electrolyte (not purged with nitrogen), followed by sequential oxidation and reduction at +0.6 and −0.4 V versus Ag/AgCl using a bipotentiostat and a three-electrode configuration (Pt wire counter electrode, Ag/AgCl pellet reference electrode, and Cr/Au working electrode below the polymer film). Imaging of the polymer films was performed in the off-resonance mode with ScanAsyst Fluid silicon nitride probes from Bruker, having a nominal resonance frequency of 150 kHz, a tip radius of R = 20 nm and a spring constant of 0.7 N m^{-1} (estimated by the thermal noise method), with the deflection sensitivity of the probes calibrated by indentation on a clean sapphire substrate in the electrolyte. Measurements were performed by bringing the AFM probe in contact with the sample surface at a controlled load force of 5 nN, and 100 force curves were recorded per sample/condition. The elastic modulus E was obtained by fitting force-distance curves $F(d)$ with a linearized Hertz model using the Nanoscope Analysis 2.0 software, assuming a Poisson's ratio $\upsilon = 0.35$:

$$F = \frac{4}{3}\frac{E}{\left(1-\nu^2\right)}\sqrt{R}\,d^{3/2} \tag{5}$$

Electrochemical Quartz Crystal Microbalance (EQCM): EQCM measurements of p(g_3TT-T2) films were carried out with a QCM200 quartz crystal microbalance from Stanford Research Systems, interfaced with a Metrohm Autolab PGSTAT302N potentiostat using a three-electrode configuration (Pt wire counter electrode, Ag/AgCl reference electrode, and Au working electrode below the polymer film). Cleaned 5 MHz AT-cut Au-coated quartz crystals were loaded onto the QCM sample holder, and the absolute frequencies of each substrate F_0 were read before spin coating with polymer films and removal of excess material outside of the Au-coated area with acetone-wetted swabs. The absolute frequencies F_1 of each polymer-coated substrate in the neat state allowed calculation of the frequency change $\Delta f_1 = F_1 - F_0$. The Sauerbrey model assumes rigid films, stating that the change in mass of the adhered material Δm is proportional to the change in frequency Δf according to:[38]

$$\Delta f = -\frac{2nf_0^{\,2}}{\sqrt{\rho_q\mu_q}}\Delta m = -C_f\Delta m \tag{6}$$

where f_0 is the resonant frequency of the fundamental mode of the crystal (5 MHz), n is the harmonic number at which the crystal is driven (n = 1 for 5 MHz with a 5 MHz crystal), ρ_q is the density of quartz (2.648 g cm^{-3}) and μ_q is the shear modulus of quartz (2.947 · 10^{11} g cm^{-1} s^{-2}). These constants—f_0, n, ρ_q and μ_q—are often combined into a sensitivity factor C_f, which is 56.6 Hz cm^2 μg^{-1} for a 5 MHz quartz crystal in air. This sensitivity factor can be calibrated individually for each crystal to ensure accurate mass change quantification. A fresh sample was used for each electrolyte concentration 0.01, 0.1, and 1 M NaCl aqueous electrolyte, and the potential was cycled between −0.4 and +0.6 V versus Ag/AgCl at a scan rate of 10 mV s^{-1}. The frequency change due to swelling of the polymer film Δf_2 was monitored during oxidation/reduction cycles, and Equation (6) was used to compare the change in mass Δm with the initial mass of the film in the pristine (dry) state m_{neat} according to:

$$\frac{\Delta m}{m_{neat}} = \frac{-C\cdot\Delta f_2}{-C\cdot\Delta f_1} = \frac{\Delta f_2}{\Delta f_1} \tag{7}$$

Gravimetric cyclic voltammetry was carried out by differentiating the mass change recorded during second-cycle CV measurements against time and smoothing the obtained derivative with Origin.

EQCM with dissipation monitoring (EQCM-D) of p(g_3TT-T2) films spin-coated on a quartz crystal with a Ti/Au-coated electrode and covered by a 0.1 M NaCl aqueous electrolyte was carried out with an instrument from QSense (E4 model) using a three-electrode configuration (Pt wire counter electrode, Ag/AgCl reference electrode, and Au working electrode below the polymer film). Changes in frequency and dissipation, Δf and ΔD, during oxidation/reduction cycles were recorded at multiple harmonics, and the Sauerbrey model was used to calculate the mass changes Δm for the 3rd overtone according to:

$$\Delta m = -\frac{C\cdot\Delta f}{n} \tag{8}$$

where C = 17.7 ng s cm^{-2} is the mass sensitivity constant of a 5 MHz quartz crystal at room temperature, and n is the number of the harmonic.

Grazing-Incidence Wide-Angle X-Ray Scattering (GIWAXS): Thin films of p(g_3TT-T2) on PSS-coated glass slides were float-transferred onto porous Si frits (Sigma-Aldrich MP54751010) by submerging in a water bath. Operando GIWAXS data were collected at the Stanford Synchrotron Lightsource beamline 17–2 at 12.7 keV at an incidence angle of 0.12 degrees in an electrochemical cell that enabled bottom gating of the electrolyte, bypassing deleterious scattering.[39,40] The films were kept in a

hydrated helium environment for the duration of the experiment to avoid drying out of the electrolyte (0.1 M NaCl). Data were analyzed using custom Python scripts, and peaks were fitted using a pseudo-Voigt model. Coherence lengths were extracted from peak widths.

Statistical Analysis: All data were used as obtained from the various instruments. There was no removal of outliers. Note that in case of some nanoindentation and AFM measurements, no data were recorded, e.g., due to some measurement error, such as the tip not being in contact with the sample. Those empty values can be seen in the raw data files published in Zenodo. All modulus values correspond to the mean and standard deviation with the sample size stated in the figure legends.

Supporting Information

Supporting Information is available from the Wiley Online Library or from the author.

Acknowledgements

J.P., D.Z., Y.K., M.J., J.K., S.H.K.P., and C.M. gratefully acknowledge financial support from the European Research Council (ERC) under grant agreement no. 101043417 and the Knut and Alice Wallenberg Foundation for a Wallenberg Scholar grant (Grant No. 2021.0295). C. Musumeci would like to acknowledge support from the Swedish Research Council (2023-03651) and from the Swedish Government Strategic Research Areas in Materials Science on Functional Materials at Linköping University (Faculty Grant SFO-Mat-LiU No. 2009-00971). J.N. and H.Y. acknowledge funding from the UK Engineering and Physical Sciences Research Council (EPSRC) programme "VALUED" (Grant Reference No. EP/W031019/1). H.Y. acknowledges PhD studentship support from the China Scholarship Council (CSC) (File No. 201906150122). J.N. thanks the Royal Society for the award of a Research Professorship. The synthesis of diazirine PA was supported by the Office of Naval Research under Award No. N00014-24-1-2115. The work at Northwestern was supported by the National Science Foundation's Materials Research Science Engineering Center (NSF DMR-2308691). Z.L. acknowledges support through the National Science Foundation Graduate Research Fellowship Program under Grant No. DGE-2234667. This research utilized beamline 17-2 of the Stanford Synchrotron Radiation Lightsource (SSRL), SLAC National Accelerator Laboratory, which is supported by the DOE, Office of Science, Office of Basic Energy Sciences under Contract No. DE-AC02-76SF00515. The authors thank Christopher J. Takacs for beamline support and Eric Tam for help with XPS measurements.

Conflict of Interest

The authors declare no conflict of interest.

Data Availability Statement

The data that support the findings of this study are openly available from the Zenodo repository at, https://zenodo.org/records/15799667.

Keywords

conjugated polymer, elastic modulus, electrochemical oxidation, nanoindentation, organic mixed ionic-electronic conductor

Received: July 31, 2025
Revised: September 25, 2025
Published online: October 17, 2025

[1] Y. Li, N. Li, W. Liu, A. Prominski, S. Kang, Y. Dai, Y. Liu, H. Hu, S. Wai, S. Dai, Z. Cheng, Q. Su, P. Cheng, C. Wei, L. Jin, J. A. Hubbell, B. Tian, S. Wang, *Nat. Commun.* **2023**, *14*, 4488.
[2] C. F. Guimarães, L. Gasperini, A. P. Marques, R. L. Reis, *Nat. Rev. Mater.* **2020**, *5*, 351.
[3] C. T. McKee, J. A. Last, P. Russell, C. J. Murphy, *Tissue Eng. Part B Rev.* **2011**, *17*, 155.
[4] G. Singh, A. Chanda, *Biomed. Mater.* **2021**, *16*, 062004.
[5] H. Trebacz, A. Barzycka, *Biomolecules* **2023**, *13*, 574.
[6] D. C. Gao, T. P. A. van der Pol, C. Musumeci, D. Y. Tu, S. Fabiano, *Annu. Rev. Chem. Biomol. Eng.* **2025**, *16*, 293.
[7] S. H. K. Paleti, S. Haraguchi, Z. Cao, M. Craighero, J. Kimpel, Z. Zeng, P. Sowinski, D. Zhu, J. Pons i Tarrés, Y. Kim, Q. Li, J. Huang, A. Kalaboukhov, B. Mihiretie, S. Fabiano, X. Gu, C. Müller, *Macromolecules* **2025**, *58*, 3578.
[8] S. H. K. Paleti, Y. Kim, J. Kimpel, M. Craighero, S. Haraguchi, C. Müller, *Chem. Soc. Rev.* **2024**, *53*, 1702.
[9] S. E. Root, S. Savagatrup, A. D. Printz, D. Rodriquez, D. J. Lipomi, *Chem. Rev.* **2017**, *117*, 6467.
[10] B. Roth, S. Savagatrup, N. V. de los Santos, O. Hagemann, J. E. Carlé, M. Helgesen, F. Livi, E. Bundgaard, R. R. Søndergaard, F. C. Krebs, D. J. Lipomi, *Chem. Mater.* **2016**, *28*, 2363.
[11] R. X. Xie, R. H. Colby, E. D. Gomez, *Adv. Electron. Mater.* **2018**, *4*, 1700356.
[12] S. Zokaei, D. Kim, E. Järsvall, A. M. Fenton, A. R. Weisen, S. Hultmark, P. H. Nguyen, A. M. Matheson, A. Lund, R. Kroon, M. L. Chabinyc, E. D. Gomez, I. Zozoulenko, C. Müller, *Mater. Horiz.* **2022**, *9*, 433.
[13] I. Abdel Aziz, J. Gladisch, C. Musumeci, M. Moser, S. Griggs, C. J. Kousseff, M. Berggren, I. McCulloch, E. Stavrinidou, *Mater. Horiz.* **2024**, *11*, 2021.
[14] C. Cendra, A. Giovannitti, A. Savva, V. Venkatraman, I. McCulloch, A. Salleo, S. Inal, J. Rivnay, *Adv. Funct. Mater.* **2019**, *29*, 1807034.
[15] M. Moser, J. Gladisch, S. Ghosh, T. C. Hidalgo, J. F. Ponder, R. Sheelamanthula, Q. Thiburce, N. Gasparini, A. Wadsworth, A. Salleo, S. Inal, M. Berggren, I. Zozoulenko, E. Stavrinidou, I. McCulloch, *Adv. Funct. Mater.* **2021**, *31*, 2100723.
[16] S. Zokaei, R. Kroon, J. Gladisch, B. D. Paulsen, W. Sohn, A. I. Hofmann, G. Persson, A. Stamm, P. O. Syrén, E. Olsson, J. Rivnay, E. Stavrinidou, A. Lund, C. Müller, *Adv. Sci.* **2021**, *8*, 2002778.
[17] J. Gladisch, E. Stavrinidou, S. Ghosh, A. Giovannitti, M. Moser, I. Zozoulenko, I. McCulloch, M. Berggren, *Adv. Sci.* **2020**, *7*, 1901144.
[18] X. Wang, K. Chen, L. S. de Vasconcelos, J. He, Y. C. Shin, J. Mei, K. Zhao, *Nat. Commun.* **2020**, *11*, 211.
[19] T. Shoa, T. Mirfakhrai, J. D. W. Madden, *Synth. Met.* **2010**, *160*, 1280.
[20] H. Lv, L. Li, M. Sun, Y. Zhang, L. Chen, Y. Rong, Y. Li, *Stem Cell Res. Ther.* **2015**, *6*, 103.
[21] A. Guo, B. Wang, C. Lyu, W. Li, Y. Wu, L. Zhu, R. Bi, C. Huang, J. J. Li, Y. Du, *Cell Regen.* **2020**, *14*, 36.
[22] M. Craighero, J. Guo, S. Zokaei, S. Griggs, J. Tian, J. Asatryan, J. Kimpel, R. Kroon, K. Xu, J. S. Reparaz, J. Martín, I. McCulloch, M. Campoy-Quiles, C. Müller, *ACS Appl. Electron. Mater.* **2024**, *6*, 2909.
[23] C. M. Cardona, W. Li, A. E. Kaifer, D. Stockdale, G. C. Bazan, *Adv. Mater.* **2011**, *23*, 2367.
[24] A. A. Mohapatra, W. K. Yual, Y. Zhang, A. A. Samoylov, J. Thurston, C. M. Davis, D. P. McCarthy, A. D. Printz, M. F. Toney, E. L. Ratcliff, N. R. Armstrong, A. L. Greenaway, S. Barlow, S. R. Marder, *Chem. Commun.* **2024**, *60*, 988.
[25] S. A. Paniagua, A. J. Giordano, O.' L. Smith, S. Barlow, H. Li, N. R. Armstrong, J. E. Pemberton, J. L. Brédas, D. Ginger, S. R. Marder, *Chem. Rev.* **2016**, *116*, 7117.
[26] G. Li, T. V. Nykaza, J. C. Cooper, A. Ramirez, M. R. Luzung, A. T. Radosevich, *J. Am. Chem. Soc.* **2020**, *142*, 6786.

[27] J. Brunner, H. Senn, F. M. Richards, *J. Biol. Chem.* **1980**, *255*, 3313.
[28] A. Savva, C. Cendra, A. Giugni, B. Torre, J. Surgailis, D. Ohayon, A. Giovannitti, I. McCulloch, E. Di Fabrizio, A. Salleo, J. Rivnay, S. Inal, *Chem. Mater.* **2019**, *31*, 927.
[29] B. Ding, I.-Y. Jo, H. Yu, J. H. Kim, A. V. Marsh, E. Gutiérrez-Fernández, N. Ramos, C. L. Rapley, M. Rimmele, Q. He, J. Martín, N. Gasparini, J. Nelson, M. H. Yoon, M. Heeney, *Chem. Mater.* **2023**, *35*, 3290.
[30] J. Hynynen, D. Kiefer, L. Yu, R. Kroon, R. Munir, A. Amassian, M. Kemerink, C. Müller, *Macromolecules* **2017**, *50*, 8140.
[31] I. P. Maria, S. Griggs, R. B. Rashid, B. D. Paulsen, J. Surgailis, K. Thorley, V. N. Le, G. T. Harrison, C. Combe, R. Hallani, A. Giovannitti, A. F. Paterson, S. Inal, J. Rivnay, I. McCulloch, *Chem. Mater.* **2022**, *34*, 8593.
[32] S. N. Patel, A. M. Glaudell, K. A. Peterson, E. M. Thomas, K. A. O'Hara, E. Lim, M. L. Chabinyc, *Sci. Adv.* **2017**, *3*, 1700434.
[33] J. Rivnay, S. Inal, B. A. Collins, M. Sessolo, E. Stavrinidou, X. Strakosas, C. Tassone, D. M. Delongchamp, G. G. Malliaras, *Nat. Commun.* **2016**, *7*, 11287.
[34] V. Untilova, H. Zeng, P. Durand, L. Herrmann, N. Leclerc, M. Brinkmann, *Macromolecules* **2021**, *54*, 6073.
[35] J. Kimpel, Y. Kim, J. Asatryan, J. Martín, R. Kroon, C. Müller, *Chem. Sci.* **2024**, *15*, 7679.
[36] J. Kimpel, Y. Kim, H. Schomaker, D. R. Hinojosa, J. Asatryan, J. Martín, R. Kroon, M. Sommer, C. Müller, *Sci. Adv.* **2025**, *11*, adv8168.
[37] W. C. Oliver, G. M. Pharr, *J. Mater. Res.* **1992**, *7*, 1564.
[38] A. D. Easley, T. Ma, C. I. Eneh, J. Yun, R. M. Thakur, J. L. Lutkenhaus, *J. Polymer Sci.* **2022**, *60*, 1090.
[39] B. D. Paulsen, A. Giovannitti, R. Wu, J. Strzalka, Q. Zhang, J. Rivnay, C. J. Takacs, *Small* **2021**, *17*, 2103213.
[40] T. J. Quill, G. LeCroy, D. M. Halat, R. Sheelamanthula, A. Marks, L. S. Grundy, I. McCulloch, J. A. Reimer, N. P. Balsara, A. Giovannitti, A. Salleo, C. J. Takacs, *Nat. Mater.* **2023**, *22*, 362.